Faraday
Discussions

Accepted Manuscript

**Faraday
Discussions**

**Royal Society of
Chemistry**

ROYAL SOCIETY
OF CHEMISTRY

ROYAL SOCIETY
OF CHEMISTRY

www.rsc.org/faraday_d

Journal Name

ARTICLE

Effect of Electrochemical dissolution and deposition order on lithium dendrite formation: a top view investigation

Wenjun Li[1, ‡], Hao Zheng[1, ‡], Geng Chu[1], Fei Luo[1], Jieyun Zheng[1], Dongdong Xiao[1], Xing Li[2], Lin Gu[1,*], Hong Li[1,*], Xianlong Wei[2], Qing Chen[2], Liquan Chen[1]

Rechargeable metallic lithium batteries are the final solutions of electrochemical storage due to their high theoretical energy densities. One of the key technological challenges is to control the morphology of metallic lithium electrode during electrochemical dissolution and deposition. Here we have investigated the morphology change of metallic lithium electrode after charging and discharging in nonaqueous batteries by *ex situ* SEM technique from top view. Formation of the hole structure after lithium dissolution and the filling of dendrite-like lithium into the holes have been observed for the first time. In addition, an *in situ* SEM investigation using an all-solid Li/Li$_2$O/super aligned carbon nanotube set-up indicates that lithium ions could diffuse across through the surface oxide layer and grow dendrite lithium after applying external electric field. The growth of lithium dendrite can be guided by electron flow when formed lithium dendrite touches the carbon nanotube.

Introduction

High energy density rechargeable battery is the key technology to support rapid developments of many emerging technologies, such as advanced portable and wearable electronic devices, electrical vehicles, smart grid, tool and toy, robot, back-up batteries for various applications. According to thermodynamic calculations, Li-O$_2$ battery has the highest theoretical gravimetric energy densities among chemical energy storage devices.[1] For the similar chemical reaction, the battery with lithium anode has the highest energy density than any other battery with different metal anode, such as Mg, Al, Na, Zn. In addition, rechargeable metallic lithium batteries (RMLB) have much higher energy densities than lithium ion batteries (LIB) with the same cathode.[1] Recently, developing RMLB have attracted increasing attentions after the first wave in 1970's, especially on Li-S, Li-air, all solid lithium batteries (ASLB) using polymer or ceramic as electrolytes.[2-6] However, periodic dissolution and deposition of metallic lithium during cycling leads to the formation of microstructured or nanostructured lithium with different morphologies, such as needle-like, dendrite, granular and mossy lithium. The newly formed structured lithium reacts significantly with nonaqueous electrolyte electrochemically and chemically[7-8]. The side products are electronic insulating and ionic conducting solid electrolyte interphase (SEI) films. The formation of SEI is unavoidable in nonaqueous lithium batteries, leading to the irreversible consumption of electrolyte and isolating of active lithium. Consequently, coulombic efficiency of the battery is decreased and the cyclic performance is poor. In addition, structured lithium becomes more dangerous and could cause internal short circuit, rapid heating and explosion of the battery.[7-9]

Several strategies have been paid to control the morphology of metallic lithium electrode during cycling, including tuning solvent and salt, ionic liquid, functional additives for modifying SEI or suppressing lithium dendrite or tuning local electrical field, lithium surface coating, solid electrolyte, ceramic separator, 3D current collector, using lithium powder instead of lithium foil, mechanical pressing.[8] In spite of great efforts on improving the performances of metallic lithium electrode, investigation on the morphology and surface composition are quite challenge due to soft and air-sensitive feature of lithium electrode. *Ex situ* and *in situ* scanning electronic microscopy (SEM) has been used widely to investigate lithium dendrite in lithium nonaqueous batteries,[10-12] and lithium polymer batteries. [13-15] Atomic force microscopy[16, 17], optical spectroscopy[18], magnetic resonance imaging (MRI) technology,[19] have also been used to investigate the morphology change of lithium electrode. *In situ* NMR was also developed successfully to quantify the amount of dendritic/mossy Li by analyzing the change in the NMR signal intensity of the Li metal during cycling.[20] Fourier transmission infrared spectroscopy (FTIR), [11, 21-22] X-ray photoelectronic spectroscopy (XPS),[22-24] Raman spectroscopy, [25-26] and secondary ion mass spectroscopy (SIMS)[22] have been used to identify the surface composition on reacted lithium electrode. Electrochemical impedance spectroscopy (EIS) and cyclic voltammetry (CV) have been performed to analyze the electrical response of the lithium electrode.[11, 16]

For the rechargeable lithium battery with cathode containing lithium source, such as Li/LiCoO$_2$ cell, the deposition of lithium occurs firstly during the first charging then follow the dissolution of lithium during discharging. In the case of rechargeable lithium battery with lithium anode as lithium source, such as Li-S, Li-air batteries, the dissolution of lithium occurs firstly during the first discharging then follows the deposition. There are no reports to distinguish the effect

of the order of dissolution and deposition on the morphology of the lithium electrode. In this work, we have investigated the order effect of dissolution and deposition by comparing the morphology change of the metallic lithium electrodes in Li/Si cell, Li/LiCoO$_2$ and Li/LiFePO$_4$ cells respectively. It is obvious that the top view is favorable to investigate the morphology change of lithium electrode. There are very few top-view SEM images of reacted lithium since lithium electrode is soft and the sample transfer could change the morphology completely. In order to solve this problem, a special stainless steel sample holder was designed. Soft lithium sheet can be embedded into the hole of the SS substrate and the surface of lithium can be flattened by mechanical pressing. The transfer of lithium electrode has been performed by touching the hard edge part of SS sample holder. In addition, our Hitachi SEM instrument has a special designed sealed sample transfer box, which allows the transfer of the air-sensitive sample from the Ar-filled glove box to the vacuum chamber of the SEM microscope without exposure to air.

Experimental

Flatten lithium sheet for this study: the lithium sheet (4 mm in diameter, 0.45 mm in thickness) in the SS sample holder was pressed by a precisely polished stainless steel pillar to flatten its surface. The roughness of the lithium foil before and after pressing was measured by a MultiMode 8 (BRUKER) scanning probe microscope (SPM) equipped in an Ar-filled glove box.[27] Atomic force microscope (AFM) image is shown in Fig. 1. The surface roughness is defined by root-mean-squared (RMS) values calculated from the AFM images.[27] As shown in Fig.1 and Table 1, the surface roughness of the pressed lithium foil is much smaller than the unpressed one. Therefore, the pressed lithium sheet is suitable for the top-view investigation.
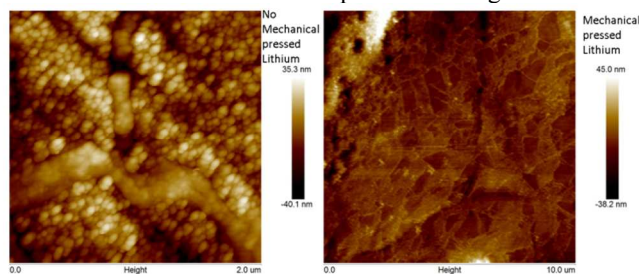
Fig. 1 The roughness of the lithium foil before and after mechanical pressing, measured by AFM.

Table 1 lithium roughness parameter before and after mechanical pressing

parameter	Ra(nm)	Rq(nm)	Roughness Rmax(nm)
Before press	8.02	10.0	72.7
After press	3.15	3.99	34.57

Electrochemical cell: a flooded two-electrode nonaqueous cell and a special designed sample holder were used and shown in Fig. 2, which can be easily assembled and disassembled and can avoid direct touching the surface of the reacted lithium electrode. Our new design is especially suitable for the sample transferring from the glove box to the *ex situ* SEM measurements. Three types of cells were assembled with surface flatten lithium sheet electrode. The cathode was the silicon/carbon (Si/C) composite electrode, LiCoO$_2$ electrode

and LiFePO$_4$ electrode respectively. All cathodes were composed of the active material, the conductive additive (carbon black) and the Polyvinylidene fluoride (PVDF) binder at weight ratio of 92:3:5. These electrodes were prepared by spreading the active material slurry on the current collector (copper foils for the Si/C composites, Al foils for LiCoO$_2$ and LiFePO$_4$). Commercial electrolytes of 1M LiPF$_6$ dissolved in ethylene carbonate-dimethyl carbonate (EC-DMC) (1:1 in v/v) without any additives were used in all cells.
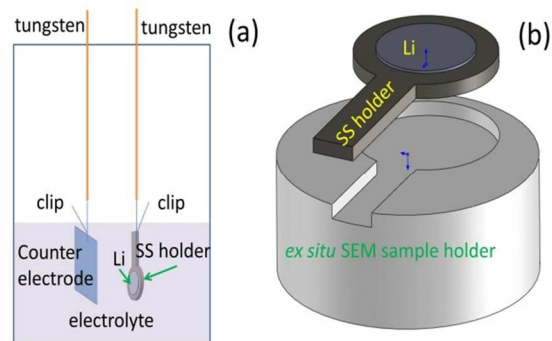
Fig. 2 Sketch of (a) a flooded two-electrode nonaqueous cell (b) sample holder for SEM investigation.

***Ex situ* SEM investigation**: As the cell was assembled, it was discharged or charged. After the discharge or charge, the cell was disassembled in the glove box and the reacted lithium foil was taken out from the cell and washed with dimethyl carbonate (DMC). The washed lithium electrode was dried in the vacuum chamber of the glove box for at least 6 hours before it was transferred to the SEM chamber of a Hitachi S4800 microscope. The special designed transfer box was used to transfer the sample, which avoid exposure of the sample to the air. In addition, a special SEM sample holder was designed to fix the installed position of the sample, which was suitable for finding the same position of the same reacted lithium electrode during each *ex situ* SEM investigation. After the SEM measurements, the lithium electrode was assembled into the cell again to be discharged or charged to next state. Such procedure was repeated, as shown in Fig.3.
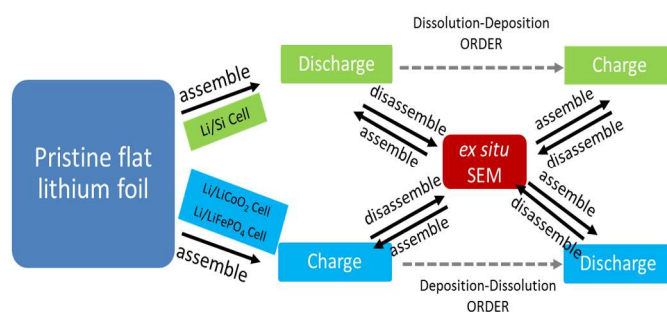
Fig. 3 The experimental design for the dissolution-deposition order and the deposition-dissolution order investigation

Order of discharging and charging of lithium electrode: The Li/Si cell was discharged firstly. Consequently, dissolution of lithium from the lithium electrode will occur firstly. The Li/LiCoO$_2$ and Li/LiFePO$_4$ cell were charged firstly. Therefore, deposition of lithium on the counter lithium electrode will

occur firstly. Accordingly, we could investigate the effect of changing the discharging/charging order on the morphology change of metal lithium electrodes. The corresponding experimental details were listed in Table. 2.

Table 2 The sample details of the *ex situ* SEM measurements

Cell	Charge/Discharge state	Charge/Discharge capacity (mAh)	SEM images
Li/Si	Dis. to 20 mV	1.33	Fig. 6 (a)
	Dis. to 5 mV	1.47	Fig. 6 (b)
	Charge to 1 V	0.42	Fig. 6 (c)
	Dis. to 5 mV	1.40	Fig. 6 (d)
Li/LiCoO$_2$	Charge to 4.2 V	3.6	Fig. 8 (c,d)
	Dis. to 3 V	1.78	Fig. 8 (e,f)
Li/LiFePO$_4$	Charge to 4 V	0.26	Fig. 9 (c,d)
	Dis. to 2.8 V	0.15	Fig. 9 (e,f)

Second ion mass spectroscopy (SIMS) experimental: All mass spectroscopy and elemental SIMS mapping (ESM) were recorded by the Hiden SIMS Workstation to analyze the composition of the lithium electrode surface after cycling. Ar ion gun was used. Full mass spectra were recorded using 1 nA ion current and the depth profiles were recorded using 100 nA ion current. ESM was recorded using 10 nA ion current. Two kinds of lithium foils, i.e. the pristine lithium foil, the lithium foil from the Li/LiFePO$_4$ battery at the second and 5th discharge state, were chosen for surface composition analysis. The sample transfer process was protected by the glove bag filled with argon.

***In situ* SEM investigation:** An all-solid-state cell was used and investigated in a FEI Quanta 600 microscope, as shown in Fig. 4. The formation and growth of the lithium dendrite were investigated. In order to construct the *in situ* micro-scale all-solid-state battery setup, two tips including one Au tip and one tungsten tip were installed on the probe workstation (Kleindiek) as shown in Fig. 4. Before closing the chamber, a piece of commercial lithium foil was stuck to tungsten tip, and the super-aligned carbon nanotube (SACNT) was attached on the Au tip. The lithium metal on tungsten tip was oxidized in the air naturally before it is transferred to the chamber. After the chamber is closed and evacuated to about 10^{-2} Pa, the tips can be moved in three dimensions by handling the manipulator, once the SACNT on Au tip was moved to contact with the surface of the native oxide layer, the *in situ* battery was constructed. The SACNT on Au tip, the native oxide layer Li$_2$O[28] and the lithium metal on tungsten tip worked as the cathode, the solid state electrolyte and the anode, respectively. In order to induce the lithium dendrite, a bias of -3 V was applied on the SACNT vs. Li metal.
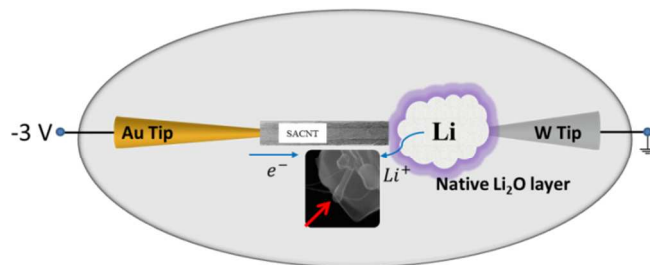
Fig. 4. The schematic illustration of the *in situ* SEM setup of all-solid-state battery. The SACNT, native Li$_2$O layer and Li metal worked as the cathode, solid-electrolyte and anode respectively. -3 V was applied on SACNT *vs.* Li metal to induce the formation of the lithium dendrite.

Results and Discussions

SEM image of original lithium sheet electrode
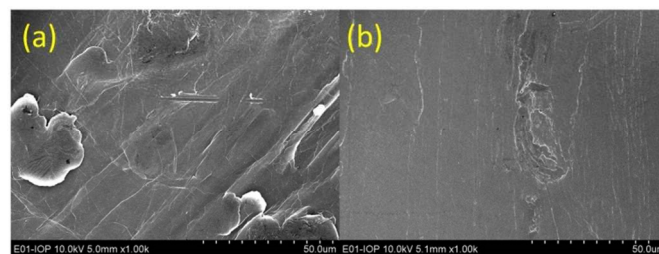
Fig.5 (a): original lithium foil, (b) flatten lithium foil

As shown in Fig.5, it is quite clear that lithium sheet after flattening treatment does have flat surface and defect structure is decreased, which is suitable for further SEM and AFM investigation. In this work, all lithium sheet electrodes used for AFM and SEM studies are flattened lithium sheet electrode embedded into the SS sample holder shown in Fig.2. For simplicity, name of lithium electrode will be used in later sections without extra description.

Morphology change of Li electrode in Li/Si cell

Fig. 6a shows a typical SEM image of the lithium electrode after the first discharge to 20 mV in the Li/Si cell. Many holes with different size and depth can be observed. In this image, the diameter of the biggest hole is about 100 μm, and the depth of the hole cannot be measured. The appearance of such large hole indicates that the electrochemical dissolution of lithium occurs more easily at the etched area. It is reasonable since the surface of the lithium electrode is covered by a layer of insulating SEI film unevenly once lithium electrode is soaked and discharged in the electrolyte. Once the lithium electrode starts to dissolve in certain area after discharging, some areas will be etched and the SEI surface layer covered on those areas can also be peeled off. The exposed fresh areas of the lithium electrode have lower resistance compared to unreacted areas and are more easily to be etched further. It is noticed that further discharge to 5 mV seems not change too much in the morphology of lithium electrode, compared to the lithium electrode discharged to 20 mV, as shown in Fig.6 (b). Some small holes can be seen clearly at the bottom inside the biggest hole and in some other regions as well.

Fig. 6 (c) shows the morphology of the lithium electrode after the first charge to 1.0 V. It can be seen that the mossy-like lithium deposits back into the biggest hole of the lithium electrode which was formed during discharging mainly. We did not observe that lithium is deposited on the flat surface of the lithium electrode during charging. It indicates that once the holes are formed, that area becomes more electrochemically active than the unreacted flatten areas.

Fig. 6 (d) shows the morphology of the lithium electrode after the second discharge to 5 mV. The morphology does not change too much and the filled mossy-like lithium in the big hole still exists but the amount decreases. The edge part of the big hole is destroyed slightly. At high magnification in Fig.6e and 6f, it can be observed clearly that the mossy-like lithium has the dendrite appearance. The diameter is about 400 nm in this case.
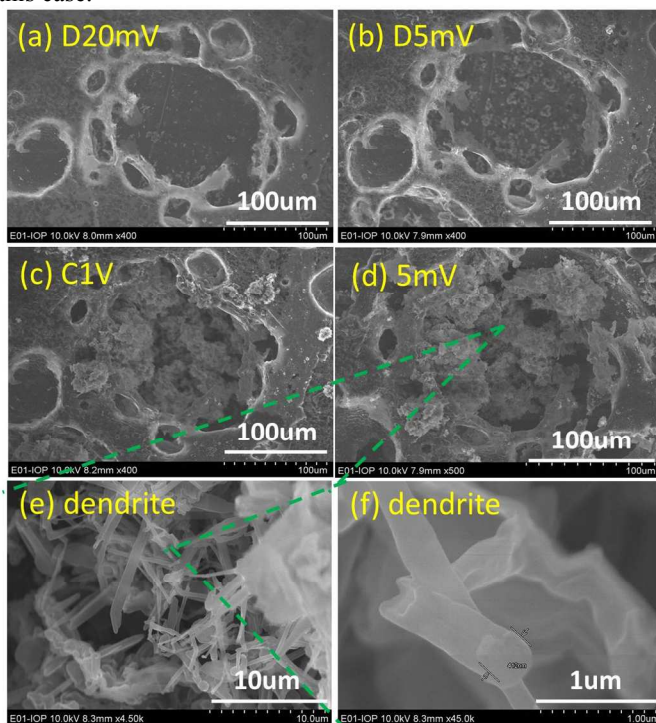
Fig. 6 Morphology evolution of the lithium electrode during lithium dissolution and deposition in the Li/Si cell. Current density for charging and discharging was 6.4 mA/cm^2 (a) 1st discharge to 20 mV
(b) 1st discharge to 5mV (c) 1st charge to 1V (d) 2nd discharge to 5 mV (e, f) SEM images of the dendrite-like lithium which deposited in the hole

For getting a whole impression, low resolution images of the lithium electrode in the Li/Si cell at different states are shown in Fig.7. In the center area of the lithium electrode, many holes can be seen clearly after the first discharging to 20 mV. The distribution of the holes is random. The hole size is about 50-100 μm. The density and size of the holes increase after further discharging to 5 mV. Some holes have merged together. At the edge part, it is noticed that dendrite-like lithium is observed, as shown in Fig.7b and 7c. After the second discharge, the surface becomes rough significantly. From Fig.7d, it is quite obvious, that the many deposited mossy-like lithium are still remained on the surface of the lithium electrode, it is quite plausible that

the remained deposited lithium after the second discharging become "dead" lithium.
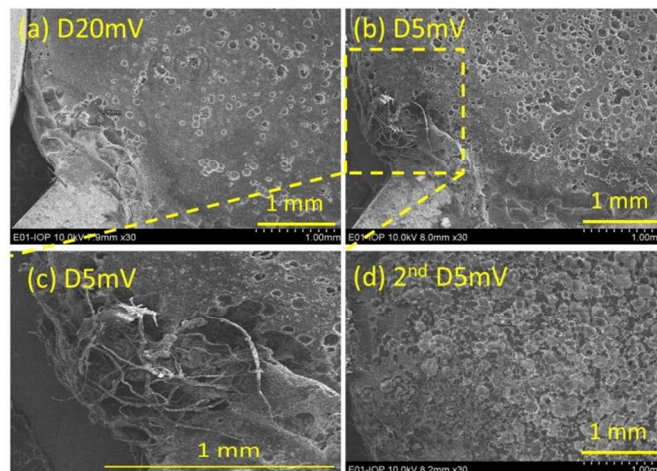
Fig. 7 evolution of lithium electrode in Li/Si system at different states (a) 1st discharge to 20 mV (b) 1st discharge to 5 mV (c) 1st discharge to 5 mV, edge part, (d) 2nd discharge to 5 mV.

The morphology evolution of the lithium electrode in the Li/LiCoO$_2$ cell is shown in Fig. 8. The pristine lithium electrode has flat surface and free of any deposited lithium.
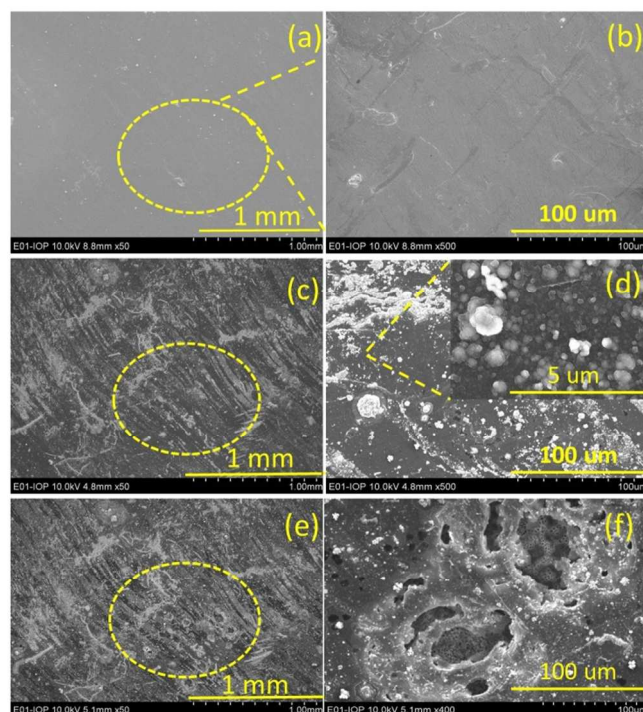
Fig. 8 Morphology evolution of the lithium electrode during lithium dissolution and deposition in the Li/LiCoO$_2$ cell. Current density for charging and discharging was 6.4 mA/cm^2. (a) pristine lithium, (b) zoomed image of the marked area of pristine lithium, (c) 1st charge to 4.2 V, (d) zoomed image of the marked area in the image (c), (e), 1st discharge to 3 V, (f) zoomed image of the marked area in the image (e).

At the charge state, the surface of the lithium electrode is covered by granular species, as shown in Fig.8c and 8d. The distribution of granular can be regarded as random, although parallel stripes can be seen. At the discharge state, most of the granular species remain. Note that the columbic efficiency of the Li/LiCoO$_2$ cell is 49% (calculated from the table 2, 1.78/3.6 = 49%), which means that only 49% deposited lithium dissolves from the lithium electrode during discharging. This calculation is consistent with the phenomena that the granular species still remain after discharge. It is also noticed that many holes appears like in Fig.6 and Fig.7. This indicates further that the hole structure is more electrochemically active than flat surface and deposited granular lithium on the surface of the lithium electrode.
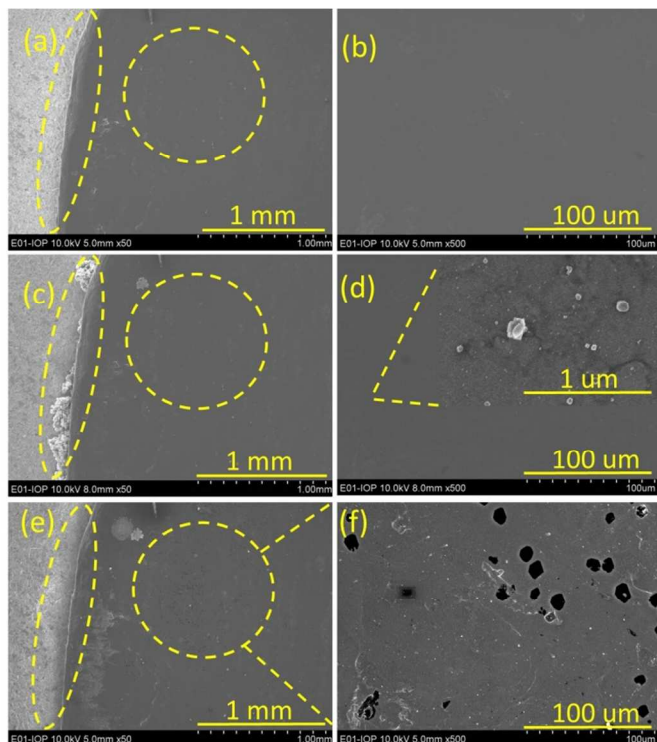
Fig. 9 Morphology evolution of the lithium electrode during lithium dissolution and deposition in the Li/LiFePO$_4$ cell. Current density for charging and discharging was 0.64 mA/cm^2. (a) pristine (b) zoomed image in marked circle area in image (a), (c) charge to 4 V, (d) zoomed image of the marked area in the image (c), (e) discharge to 2.8 V, (f) zoomed image of the marked area in the image (e)

In both cases of Li/Si cell and Li/LiCoO$_2$ cell, the current density during discharging and charging was 6.4 mA/cm^2 and the corresponding capacity for the dissolution and deposition of lithium is about 1-3 mAh. Such capacity and current density are comparable values for the discharging and charging of commercial lithium batteries. In order to study the effect of the the current density and capacity on the morphology of the lithium electrode, another Li/LiFePO$_4$ cell was tested with one tenth of the current density and the capacity of the Li/LiCoO$_2$ cell. As shown in Fig. 9c, a few granular particles can be seen on the surface of the lithium electrode after charging. After discharging, many holes with the size of 10 μm occurred accompanied with some smaller holes. These phenomena are similar as the case of Li/LiCoO$_2$ cell, but quite possibly in early stage.

Since lithium electrode has excellent electronic conductivity and ionic conductivity, the electrolyte has also high ionic conductivity and high concentration, therefore, it is not likely that the inhomogeneity of the transport of electron and lithium cations in the lithium electrode and inhomogeneous ionic flow leads to the formation of inhomogeneous hole structure and dendrite/granular/mossy like lithium. We suspect that the SEI on the lithium electrode plays the key role to influence the morphology of the lithium electrode during electrochemical dissolution and deposition in nonaqueous lithium cells. However, it is not very easy to detect the homogeneity of the SEI on the lithium electrode. We performed SIMS to investigate this issue indirectly.

SIMS investigation on surface compositions

With the sample holder, it is convenient to scan the negative ion full mass spectroscopy of pristine and reacted lithium electrode by SIMS technique. The lithium electrode after five cycles in a Li/LiFePO$_4$ cell is detected and the full negative ion mass spectrum is shown in Fig. 10.
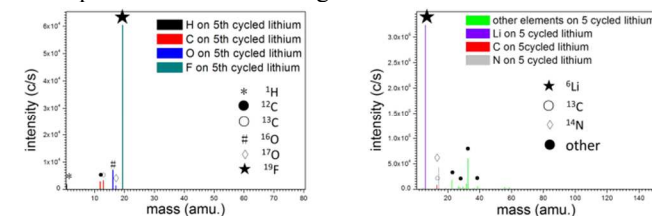
Fig. 10 SIMS full negative ion mass scanning spectrum (Left) and positive ion spectrum (Right) of the lithium electrode after 5 cycles. The current density was 0.64 mA/cm^2.

According to the negative ion spectroscopy, the four elements (namely H, C, O, F) in the surface can be identified. Li, C and N can be identified from the positive ion spectrum. Accordingly, the SIMS results are consistent with previous investigations, which demonstrated that the SEI on the surface of lithium electrode contains Li$_2$CO$_3$, LiF, Li$_2$O.[29-31]
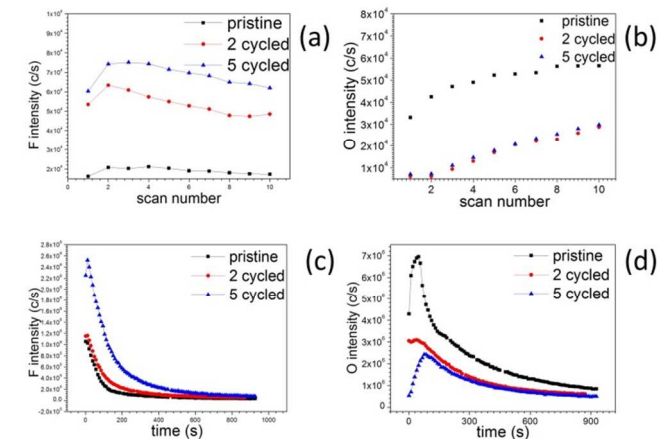
Fig . 11 The surface depth distribution of (a) fluorine, (b) oxygen and element depth profile of (c) fluorine and (d) oxygen in pristine lithium electrode, after the second cycle, and the fifth cycle.

With the cycling scanning, the depth distribution of every element can be also detected. The scanning mode using a small ion beam current (1 nA) and in spot mode can only get the

depth information from the surface of the sample. In this work, a raster mode provided by the Hiden SIMS was used, which applied a bigger ion beam current (100 nA) and can reflect the depth profile more accurately. Fig. 11 shows the SIMS signals from the strongest two peaks of F and O. It can be seen that concentration of fluorine on the surface is increased significantly after cycling and the concentration of oxygen decreases. This is reasonable that LiF is gradually covered on pristine oxide layer.

The Elemental SIMS Mapping were also performed and shown in Fig.12. The element distribution on the surface of the lithium electrode is inhomogeneous. The element mapping consists with the depth profiles: the concentration of fluorine is increased and the oxygen is decreased after cycling. Accordingly, the coverage of the SEI on the lithium electrode is inhomogeneous and the out-layer is enriched with fluorine.
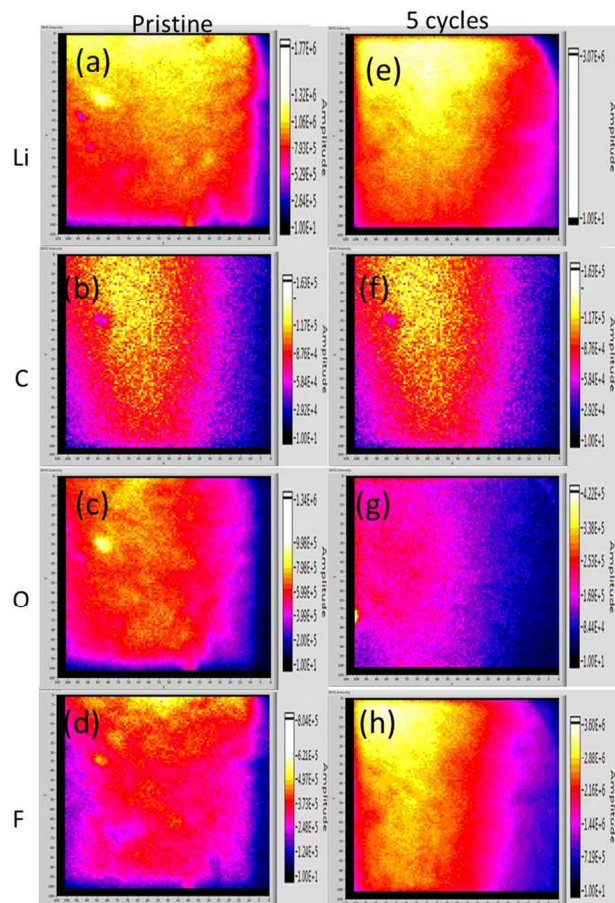
Fig. 12 ESM of Li ,F, C, O: (a), (c), (e), (g) in the pristine lithium and (b), (d), (f), (h) in the 5 cycled lithium electrode

In situ SEM investigation on the growth of lithium dendrite
Furthermore, the lithium dendrite formation has been investigated by the means of *in situ* SEM. Currently, we cannot perform *in situ* SEM investigation on liquid nonaqueous cell. We built an all-solid-state battery in the SEM chamber (See Fig.4) , with the SACNT, the native oxide layer on lithium surface, the Li metal as the cathode, solid-electrolyte and anode respectively.[32] As shown in Fig. 13, -3 V was applied on the SACNT *vs.* Li metal, to discharge the all-solid-state battery. It is observed that the lithium dendrite is formed after applying external electrical field for 700 seconds. (Fig. 13 (b)), and grew along a random direction until it overlapped the SACNT (Fig.

13a, b, c). Once the dendrite and SACNT overlapped each other, the dendrite starts to grow along the SACNT, rather than along the previous growth direction. The growth of the lithium dendrite has to be accompanied with the transportation of the lithium ion and electron. , which may be due to the high electronic conductivity of CNT. This phenomenon means that after growing to certain length, the electron flow could also guide the formation of lithium dendrite.

Actually, the whole process of the dendrite growth was followed and captured, the Fig. 13 (a, b, c, d) were just selected for demonstrating. And size evolution of the dendrite was extracted from the *in situ* captured images, as plotted in Fig. 13 (e). It is demonstrated that the growth of the dendrite was a diffusion-controlled process.

The formation of the dendrite lithium in the *in situ* SEM experiment means that the lithium ions can migrate across the surface Li_2O layer and nucleate on the top of the Li_2O covered lithium electrode and grow into the dendrite. These results consist with the appearance of the lithium dendrite of Li/Si cell during discharging (lithium extraction) shown in Fig. 7 (c). It is also interesting to notice that the diameter of the lithium dendrite remains the same (about 470 nm), the length of the dendrite increase continuously to as long as 1.72 μm (Fig. 13 (d)). Further finite element simulation is carrying out.
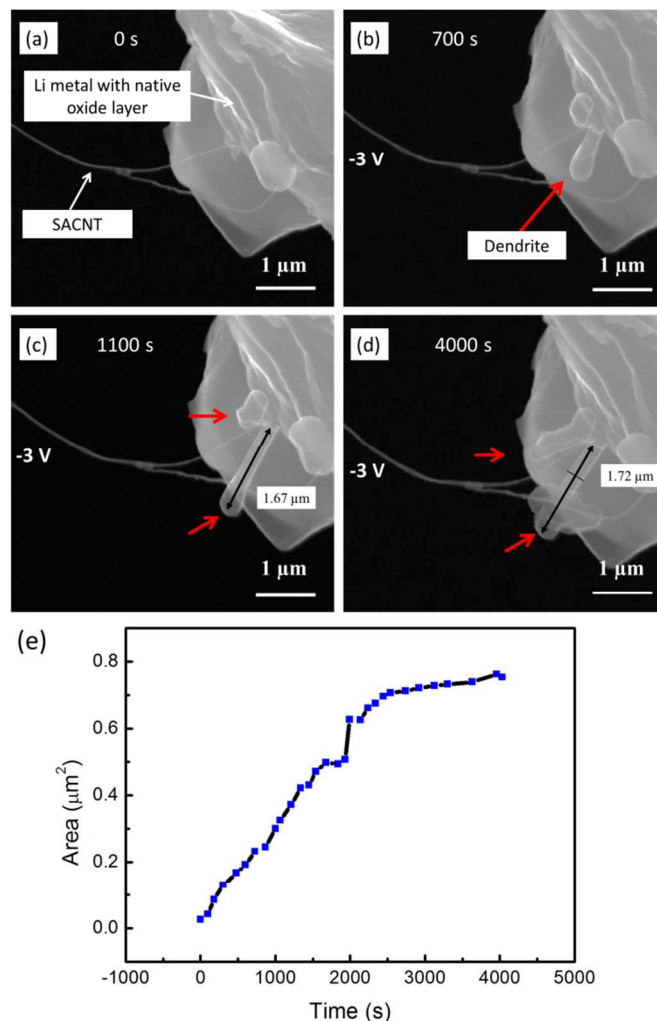
Fig. 13 The morphology evolution of the lithium dendrite in an *in situ* all-solid-state battery and the lithium dendrites were indicated by the red arrows. (a), (b), (c), (d) was the selected

morphology of the lithium dendrite, with the electrical field applied for 0 s, 700 s, 1000 s, 4000 s respectively. The increase of the cross section area of the lithium dendrite is plotted in (e).

As investigated above, in both *ex situ* SEM and *in situ* SEM, formation of dendrite like lithium can occur in both dissolution and deposition. In the case of dissolving firstly, large holes are formed randomly after delithiation and dendrite-like and mossy-like lithium preferentially fill the holes after lithiation. In the case of depositing firstly, granular-like lithium will deposit on the surface of the lithium electrode randomly after lithiation. The hole-like structure forms again on the surface in spite of covered by granular-like lithium. Since the surface of lithium electrode is covered by a layer of SEI unevenly, the dissolution and deposition of lithium are not uniformly. Whatever the charging/discharging (dissolution/deposition) order, mossy-like or granular-like lithium cannot disappear. These phenomena will definitely lead to the formation of "dead" lithium, which is not favorable for achieving good cyclic performance and high coulombic efficiency for rechargeable lithium battery.

Our report shows that top-view direct observation on the morphology of lithium electrode is now technological feasible. Combining with AFM, conducting AFM, XPS, SIMS, it is possible to understand clearly the evolution of the structure and chemical composition of the lithium electrode in rechargeable lithium batteries. Further investigations on the morphology of the lithium electrode in different lithium batteries, nonaqueous electrolytes with functional additives, surface coating with solid electrolyte and different atmosphere are carrying out. Those investigations should be essential for developing rechargeable lithium batteries.

Conclusions

Flat surface of lithium electrode with hard stainless steel sample holder is designed for *ex situ* SEM investigation. In the case of Li-Si cell, large amount of hole-like structures with 100 μm hole size and a few amount of lithium dendrite have been observed after discharging. Mossy-like and dendrite-like lithium are found mainly in the holes formed during discharging. Some of them do not disappear after the second discharge, indicating the existence of "dead lithium". In the case of $Li/LiCoO_2$ and $Li/LiFePO_4$ cells, granular like lithium is found on the surface of the lithium electrode after the first charging. Quite a lot of granular-like lithium remains after the first discharging. And hole-like structure appears again. *In situ* SEM demonstrates clearly that the lithium dendrite could grow on the surface oxide (Li_2O) covered lithium during discharging of the $Li/Li_2O/SACNT$ cell. Inhomogeneous deposition and dissolution of dendrite/mossy/granular like lithium and hole-like structures is believed to be related to inhomogeneous coverage of the SEI film, not likely to be related to the homogeneity of the electronic or ionic conductivity for lithium electrode.

Notes and references

[1] Beijing National Laboratory for Condensed Matter Physics, Institute of Physics, Chinese Academy of Sciences, Beijing, 100190, P. R. China

[2] Key Laboratory for the Physics and Chemistry of Nanodevices, Department of Electronics, Peking University, Beijing 100871, P. R. China.

‡ Wenjun Li and Hao Zheng contributed equally.

† Footnotes should appear here. These might include comments relevant to but not central to the matter under discussion, limited experimental and spectral data, and crystallographic data.

Electronic Supplementary Information (ESI) available: [details of any supplementary information available should be included here]. See DOI: 10.1039/b000000x/

1   C. X. Zu, H. Li, *Energy Environ. Sci.*, 2011, **4**, 2614; J. Y. Peng,. C. X. Zu,. H. Li, *Energy Storage Sci. Tech.*, 2013, **2**, 55.

2   M. Winter, J. O. Besenhard, M. E. Spahr, P. Novak, *Adv. Mater.* 1998, **10**, 725

3   J. M. Tarascon, M. Armand, *Nature*, 2001, **414**, 359.

4   J. B. Goodenough, Y. Kim, *Chem. Mater.* 2010, **22**, 587.

5   B. Scrosati, J. Garche, *J. Power Sources*, 2010, **195**, 2419

6   B. Dunn, H. Kamath, J. M. Tarascon, *Science*, 2011, **334**, 928

7   D. Aurbach, Nnoaqueous Electrochemistry, Marcel Dekker, New York, 1999.

8   H. Kim, G. Jeong, Y. U. Kim,c J. H. Kim, C. M. Park, H. J. Sohn, *Chem. Soc., Rev.* , 2013, **42**, 9011.

9   K. Xu, *Chem. Rev.* 2004, **104**, 4303.

10 Z. I. Takehara, K. I. Kanamura, *Electrochimica Acta.* 1993, **38**, 1169.

11 D. Aurbach, B. Markovsky, A. Shechter, and Y. Ein-E1i, J. Electrochem. Soc., 1996, 143, 3809.

12 S. Shiraishi, K. Kanamura and Z. Takehara, *Langmuir*, 1997, **13**, 3542.

13 F. Orsini, A. Du Pasquier, B. Beaudoin, J.M. Tarascon, M. Trentin, N. Langenhuizen, E. De Beer, P. Notten, *J. Power Sources* 1998, **76**, 19–29

14 C. Brissot , M. Rosso, J.N. Chazalviel , S. Lascaud, *J. Power Sources* 1999, **81–82**, 925

15 M. Dolle´, L. Sannier, B. Beaudoin, M. Trentin, J. M. Tarascon, *Electrochem. Solid-State Lett.*, 2002, **5**, A286

16 D. Aurbach , B. Markovsky, M.D. Levi, E. Levi, A. Schechter, M. Moshkovich, Y. Cohen, *J. Power Sources* 1999, **81–82**, 95

17 K. Morigaki, *J. Power Sources* 2002, **104**, 13

18 W. S. Kim, W. Y. Yoon, *Electrochimica Acta* 2004, **50**, 541

19 S. Chandrashekar, N. M. Trease, H. J. Chang, L.-S. Du, C. P. Grey, A. Jerschow, *Nat. Mater.*, 2012, 11, 311.

20 R. Bhattacharyya, B. Key, H. Chen, A. S. Best, A. F. Hollenkamp and C. P. Grey, *Nat. Mater.*, 2010, 9, 504.

21 D. Aurbach, Y. Ein-Eli, A. Zaban, *J. Electrochem. Soc.* 1994, **141**, L1.

22 D. Aurbach, M. L. Daroux, P. W. Faguy, E. Yeager, *J. Electrochem.*

Faraday Discussions Accepted Manuscript

Soc., 1988, **135**, 1863

23 K. Kanamura, S. Shiraishi and Z.-I. Takehara, *J. Electrochem. Soc.*, 1994, **141**, L108.
24 D. Aurbach, I. Weissman, A. Schechter, H. Cohen, *Langmuir* 1996, **12**, 3991.
25 M. Odziemkowski, M. Krell and D. E. Irish, *J. Electrochem. Soc.*, 1992, **139**, 3052.
26 P. C. Howlett, D. R. MacFarlane, A. F. Hollenkamp, *J. Power Sources*, 2003, **114**, 277.
27 J. Y. Zheng, H. Zheng, R. Wang, L. B. Ben, W. Lu, L. W. Chen, L. Q. Chen, H. Li, *Phys. Chem. Chem. Phys.*, DOI: 10.1039/c4cp01968g
28 X. H. Liu and J. Y. Huang, *Energy Environ. Sci.*, 2011, **4**, 3844.
29 Bates J B. *U.S. Patent* 5,314,765[P]. 1994-5-24.
30 X. Wang, Y. Hou, Y. Zhu, Y. Wu and R. Holze, *Sci. Rep.*, 2013, 3, 1401.
31 S. H. Lee, J. R. Harding, D. S. Liu, J. M. D'Arcy, Y. Shao-Horn and P. T. Hammond, *Chem. Mater.*, 2014, 26, 2579-2585.
32 N. Choi, *Solid State Ionics*, 2004, 172, 19-24.